Appl. Phys. B 68, 333–341 (1999)

Applied Physics B
Lasers
and Optics

Homodyne detection of second-harmonic generation as a probe of electric fields

J.I. Dadap[1], **J. Shan**[1], **A.S. Weling**[2], **J.A. Misewich**[3], **T.F. Heinz**[1,2]

[1] Department of Physics, Columbia University, New York, NY 10027, USA
[2] Department of Electrical Engineering, Columbia University, New York, NY 10027, USA
[3] IBM T.J. Watson Research Center, P.O. Box 218, Yorktown Heights, NY 10598, USA
(Fax: +1-212/854-1909, E-mail: tony.heinz@columbia.edu)

Received: 16 December 1998

Abstract. We demonstrate and analyze a new method for probing electric field strengths using optical second-harmonic generation. The technique, based on a homodyne detection scheme, employs interference between the field-induced second-harmonic radiation from the sample and strong second-harmonic radiation from a reference. The scheme provides a linear relationship between the measured second-harmonic signal strength and the amplitude of the electric field being probed, thus providing easy calibration of the amplitude of the electric field and direct information on its sign. Experimental results are presented for direct and homodyne detection of in-plane fields in silicon structures. A discussion of the expected signal-to-noise characteristics is presented and the results are compared to experimental findings. Homodyne detection of electric fields with strengths on the order of 100 V/cm can be achieved with reasonable integration times.

PACS: 42.65.-k; 42.65.Ky; 42.70.Nq

Optical second-harmonic generation (SHG) has been widely recognized as a surface-sensitive probe in centrosymmetric materials [1, 2]. As is well known, this sensitivity arises from the fact that the SHG process is dipole-forbidden in a centrosymmetric medium. The breaking of the inversion symmetry at a surface or interface greatly alters SHG from the sample. The same principle is operative when an electric field $\boldsymbol{E}^0$ is applied to a centrosymmetric material. The electric field $\boldsymbol{E}^0$, as a polar vector, acts to lift the inversion symmetry of the material [2]. The efficiency for SHG is thus strongly influenced and measurement of SHG provides a sensitive probe of electric fields present within the optical probing volume. The effect of an applied electric field is thus quite different from that of an applied magnetic field. The latter can alter existing SHG contributions, but, as an axial vector, does not cause the inversion symmetry of the bulk to be lifted [2].

The high sensitivity of SHG for probing of the electric fields was demonstrated early in the history of nonlinear optics. Such an electric field-induced SHG (EFISH) process was first reported by Terhune et al. [3] for a calcite sample and extended soon thereafter to semiconductors and metals by Lee et al. [4]. More recently, systematic studies of the influence of electric fields on SHG have been pursued for centrosymmetric media [5–7], as well as for certain non-centrosymmetric materials with high symmetry [8]. The EFISH process in aqueous environments has also been intensively investigated in several interesting regimes [4, 9, 10]. It has been shown to be both of fundamental interest and a useful tool for probing chemical processes at interfaces. An especially attractive feature of the EFISH process for probing electric fields lies in the possibility for measurements with extremely high time resolution. Time resolution down to the femtosecond regime can be achieved by sampling the material system with ultrafast pulses from a modelocked laser. This approach has been applied successfully to study the influence of charge-carriers on the dynamics of internal electric fields in insulators [10] and semiconductors [11, 12], and to probe microwave [13] and ultrafast transient electric fields directly in time domain [14, 15].

While the background-free character of the EFISH process in a centrosymmetric medium constitutes the principal attractive feature of the method, it also imposes certain complications and limitations. In particular, if we do indeed observe negligible SHG in the absence of the applied field $\boldsymbol{E}^0$, then we expect the induced second-harmonic (SH) polarization to vary linearly with $\boldsymbol{E}^0$. In this case, the radiated SH field will also be linear in $\boldsymbol{E}^0$. The measured quantity is, however, the SH intensity $I_{2\omega}$, which will then scale quadratically with the electric field $\boldsymbol{E}^0$ being probed. Such a quadratic relation implies both the need for careful calibration and, more importantly, the loss of information on the sign of the electric field. While the sign of $\boldsymbol{E}^0$ can be recovered from a measurement of the phase of the radiated SH field, it is clearly desirable to have an experimental methodology free of these complications. Such a method is the homodyne detection scheme presented in this paper.

The homodyne detection scheme is a well-established method in which a weak signal of interest is combined with

a strong reference (or local oscillator) signal. In an appropriate regime, the detected intensity of the superposed signal and local oscillator varies linearly with the field strength of the signal. The possibility of benefiting from homodyne detection for surface SHG was first examined explicitly by Thiansathaporn and Superfine in 1995 [16]. In the present study, we exploit the homodyne method for the measurement of electric fields through the EFISH process. For this application, the homodyne detection scheme provides a linear relationship between the experimentally measured SH intensity $I_{2\omega}$ and the electric field $\boldsymbol{E}^0$ being probed. In addition to the desired linearization of the measured response, the homodyne method may, as we discuss below, improve the signal-to-noise characteristics of the measurement.

The key element in a homodyne measurement is a strong local oscillator with which to interfere the signal of interest. In the context of an EFISH measurement, the required reference is simply an appropriate field-independent SH beam. In certain cases, it may be possible to make use of the surface dipole or bulk quadrupole SHG response of the sample itself for this purpose. This approach has, in fact, been demonstrated in studies of field-induced SHG in silicon structures [6, 13, 15]. Such an internal reference is very convenient and produces a reference beam with well-matched temporal and spatial properties. On the other hand, this approach may not be appropriate for many situations [17]. In particular, as we discuss below, optimal performance of the homodyne measurement requires a local oscillator signal with the appropriate amplitude and phase with respect to the EFISH radiation. This may be difficult to achieve with an internal reference signal because of inherent phase differences in the radiated fields, inadequate amplitude of the reference field, constraints imposed by polarization selection rules, or the like. Another method of linearizing the SH response to the electric field $\boldsymbol{E}^0$ of interest is to augment $\boldsymbol{E}^0$ by a large known electrical bias field, as has been demonstrated in the detection of microwave electrical fields in a biased semiconductor by Ohlhoff et al. [13]. While this approach is simple and effective, it is obviously restricted in its range of application.

In this paper, we present a detailed description of a general approach to the problem of homodyne detection for EFISH measurement. The method makes use of an auxiliary nonlinear crystal (quartz) for the production of the strong reference SH field [18]. We describe the appropriate methodology for controlling the amplitude and phase of this reference signal. Experimental results are presented for the detection of in-plane electric fields in a silicon structure for both the direct (background-free) and homodyne detection scheme. The linearization of the response of the SH intensity to the electric field of interest is demonstrated explicitly. We analyze the expected signal-to-noise ratios for the direct and homodyne detection schemes. Favorable characteristics are expected for the homodyne measurements under circumstances of effective interference between the EFISH and reference radiation, as well as modest noise in the probe laser. The trends of this analysis are verified by the experimental data, although the improvement predicted for ideal conditions is not fully achieved. From the signal-to-noise analysis and the experimental data, we find that electrical field strengths on the order of 100 V/cm are detectable with the homodyne scheme and reasonable integration times. Further improvements in this sensitivity may be anticipated.

1 Theoretical considerations

1.1 SH generation

Before discussing the details of the linearization technique, we first consider the different constituents of the SH polarization from a centrosymmetric sample in the presence of the electric field of interest, $\boldsymbol{E}^0$. We assume that the electric field $\boldsymbol{E}^0$ is constant within the volume generating the SH signal. In the usual limit where perturbation theory applies, we may write for the ith component of the source polarization in a sample [2],

$$P_i^{2\omega} = \chi_{s,\,ijk}^{(2)\mathrm{D}} E_j^{\omega} E_k^{\omega} \delta(z) + \chi_{ijkl}^{(2)\mathrm{Q}} E_j^{\omega} \nabla_k E_l^{\omega} + \chi_{ijkl}^{(3)} E_j^{\omega} E_k^{\omega} E_l^0 \,. \quad (1)$$

Here we denote the optical field at the fundamental frequency ω by E_i^{ω}; $\chi_{s,\,ijk}^{(2)\mathrm{D}}$ is the surface dipole response of the second-order nonlinearity; $\chi_{ijkl}^{(2)\mathrm{Q}}$ is the bulk quadrupole susceptibility tensor for SHG; and $\chi_{ijkl}^{(3)}$ is the third-order susceptibility that is responsible for EFISH. The first two terms are field-independent, while the last term is field-dependent. Both the surface dipole and bulk quadrupole terms may vanish for certain special geometries, while the field-induced terms are retained.

The magnitude of the SH field at frequency 2ω scales as the induced SH polarization given by (1) although these two vectors are, in general, not parallel [2]. In terms of the electric field $\boldsymbol{E}^0$, the SH field from the sample can be expressed as

$$\begin{aligned} E_{\mathrm{S},i}^{2\omega} &= E_{\mathrm{FI-S},i}^{2\omega} + \kappa_{ij} E_j^0 \\ &\equiv E_{\mathrm{FI-S},i}^{2\omega} + E_{\mathrm{FD},i}^{2\omega} \,. \end{aligned} \quad (2)$$

Here, $E_{\mathrm{FI-S},i}^{2\omega}$ represents the field-independent SH radiation from the sample, which arises from the first two terms in (1); $E_{\mathrm{FD},i}^{2\omega}$ describes the field-dependent SH response from the sample, which arises from the last term in (1). The tensor κ_{ij}, relating $E_{\mathrm{FD},i}^{2\omega}$ to the electric field E_j^0, depends on the input optical fields, the relevant nonlinear susceptibility $\chi_{ijkl}^{(3)}$, and the Fresnel coefficients at the fundamental and SH frequencies. Equation (2) is the most general relation between the probed electric field and the radiated SH field; it reveals the linear relation between the two fields, but allows for the fact that they need not be parallel.

We consider explicitly the case of probing a sample with the incoming fundamental beam at normal incidence to the surface. For isotropic or (100) cubic materials, the first two terms in (1) vanish [19]. The susceptibility of the remaining field-induced term has three independent tensor elements for the SHG process – $\chi_{iiii}^{(3)}$, $\chi_{iijj}^{(3)}$, and $\chi_{ijji}^{(3)}$, where the indices $\{i, j\}$ are defined with respect to the crystallographic axes. For the class of materials considered here, the SH field from the sample is proportional to the polarization, i.e., $E_{\mathrm{S},i}^{2\omega} \propto P_i^{2\omega}$. The field-dependent SH field along a crystallographic axis i, for example in the case of an isotropic or a cubic (100) surface, is given by

$$E_{\mathrm{FD},i}^{2\omega} \propto \chi_{iiii}^{(3)} \left(E_i^{\omega}\right)^2 E_i^0 + \chi_{ijji}^{(3)} \left(E_j^{\omega}\right)^2 E_i^0 + 2\chi_{ijij}^{(3)} E_j^{\omega} E_i^{\omega} E_j^0 \,. \quad (3)$$

If the polarization of the fundamental optical field is aligned with one of the in-plane crystallographic axes, (3) yields

$$E_{\mathrm{FD},i}^{2\omega} \propto \chi_{iiii}^{(3)} \left(E_i^{\omega}\right)^2 E_i^0 \quad (3a)$$

and

$$E^{2\omega}_{\mathrm{FD},i} \propto \chi^{(3)}_{ijji} \left(E^{\omega}_{j}\right)^2 E^{0}_{i} \,. \tag{3b}$$

Hence by applying either of the above expressions, one can probe the vector nature of the electric field using SHG. When these measurements are performed in combination with the linearization scheme and an appropriate calibration, the amplitude and direction of the electric field along the surface can be conveniently obtained. A more general analysis of the vector characterization of electric fields, including consideration of the out-of-plane component of the field will be presented elsewhere.

In this study, we have employed input and output polarizations that are both *s*-polarized in a near normal-incidence geometry. Even at incidence angles $> 0°$, for this polarization configuration, the surface dipole term of (1) vanishes (in isotropic or (100) cubic materials) [19]. For this same geometry, the bulk quadrupole term is also absent (provided the input fields are along the (100) surface crystallographic axes) [19]. Hence the total SH field from the sample arises only from the field-dependent contribution and is still given by the simple expression of (3a). Thus, the EFISH field for the *s*-in/*s*-out polarization configuration of our measurement yields a response proportional to the projection of the field $\boldsymbol{E}^0$ along the $\hat{\boldsymbol{s}}$ direction, i.e., $\boldsymbol{E}^0 \cdot \hat{\boldsymbol{s}}$. To maximize our sensitivity to the applied field $\boldsymbol{E}^0$, we choose to orient $\boldsymbol{E}^0$ along the $\hat{\boldsymbol{s}}$, i.e., $\boldsymbol{E} = E^0 \hat{\boldsymbol{s}}$.

1.2 Homodyne detection

We now describe the scheme for linearizing the response of the total SH signal with respect to the electric field. For generality, consider the case where the sample has an intrinsic field-independent contribution to the total SHG. Denote the total field-independent SH field as $\boldsymbol{E}^{2\omega}_{\mathrm{FI}} = \boldsymbol{E}^{2\omega}_{\mathrm{FI-S}} + \boldsymbol{E}^{2\omega}_{\mathrm{FI-R}}$, where $\boldsymbol{E}^{2\omega}_{\mathrm{FI-S}}$ and $\boldsymbol{E}^{2\omega}_{\mathrm{FI-R}}$ are the background and reference fields generated by the sample and external sources, respectively. Assuming that these fields have the same spatial distribution and polarization, we obtain the total intensity, $I_{2\omega} \propto |\boldsymbol{E}^{2\omega}_{\mathrm{T}}|^2$, with $\boldsymbol{E}^{2\omega}_{\mathrm{T}} = \boldsymbol{E}^{2\omega}_{\mathrm{FD}} + \boldsymbol{E}^{2\omega}_{\mathrm{FI}}$:

$$I_{2\omega} \propto \left|\boldsymbol{E}^{2\omega}_{\mathrm{FD}}\right|^2 + \left|\boldsymbol{E}^{2\omega}_{\mathrm{FI}}\right|^2 + 2E^{2\omega}_{\mathrm{FD}} \left|\boldsymbol{E}^{2\omega}_{\mathrm{FI}}\right| \cos\varphi \,. \tag{4}$$

In the expression above and in the discussion hereafter, we take $E^{2\omega}_{\mathrm{FD}}$ as a real quantity. The angle φ is then defined to be the phase difference between the EFISH signal $\boldsymbol{E}^{2\omega}_{\mathrm{FD}}$ and the field-independent response $\boldsymbol{E}^{2\omega}_{\mathrm{FI}}$ for a specified applied electric field $\boldsymbol{E}^0$.

If the reference field is much larger than the signal field, i.e., $|\boldsymbol{E}^{2\omega}_{\mathrm{FI}}| \gg |\boldsymbol{E}^{2\omega}_{\mathrm{FD}}|$, then

$$I_{2\omega} \propto \left|\boldsymbol{E}^{2\omega}_{\mathrm{FI}}\right|^2 + 2E^{2\omega}_{\mathrm{FD}} \left|\boldsymbol{E}^{2\omega}_{\mathrm{FI}}\right| \cos\varphi \,. \tag{4a}$$

Since $E^{2\omega}_{\mathrm{FD}} \propto E^0$, it becomes clear from (4a) that, provided $\varphi \neq \pi/2$ total SH intensity $I_{2\omega}$ (a) depends linearly on the electric field E^0, and (b) yields the sign information of E^0.

To linearize the signal by the homodyne detection scheme, we may rely on any SH signal of appropriate amplitude and phase. If the field-independent signal from the sample itself is relatively strong and exhibits a relative phase with respect to the field-induced signal near 0 or π, then an auxiliary reference may not be necessary. Such was the case in the study of Nahata and Heinz [15], in which the authors used the surface SH dipole radiation to linearize the response to the terahertz electric field. In the present case as mentioned above, we have employed special geometries in which the field-independent SH response of the sample is absent, i.e., $\boldsymbol{E}^{2\omega}_{\mathrm{FI-S}} = 0$.

To supply the required field-independent SH radiation, we used a quartz crystal located along the probe laser beam path before the sample. By employing the dispersion between the fundamental and SH beams in air, we can vary the relative SH phase between the quartz reference and the sample by changing their relative separation L. The corresponding phase difference is simply given by

$$\Delta\varphi_{\mathrm{air}} = \frac{2\omega}{c} \Delta n L \,, \tag{5}$$

where $\Delta n = n(2\omega) - n(\omega)$ is the difference in the refractive indices of air at the SH and fundamental frequencies. A direct calculation of the oscillation period using the published refractive index of air [20] yields $\Delta L = 46\,\mathrm{mm}$ for the fundamental wavelength of $\lambda = 770\,\mathrm{nm}$ relevant for our experiments.

The amplitude of the SH field from the quartz reference, after passing through an analyzer, can also be adjusted. This is accomplished by rotating the crystal about its surface normal. We may develop this idea more explicitly by taking into account the 32 point-group symmetry of the quartz crystal. For normal incidence excitation of a *z*-cut crystal, we access only a single independent element of the nonlinear optical susceptibility tensor, $\chi^{(2)}_{x'x'x'}$, where x' is a crystallographic axis [21]. The components of the SH field from the quartz reference in the laboratory frame are found to be

$$\begin{pmatrix} E^{2\omega}_{\mathrm{FI-R},x} \\ E^{2\omega}_{\mathrm{FI-R},y} \end{pmatrix} \propto \begin{bmatrix} \cos 3\theta & -\cos 3\theta & \sin 3\theta \\ \sin 3\theta & -\sin 3\theta & -\cos 3\theta \end{bmatrix} \begin{bmatrix} \left(E^{\omega}_{x}\right)^2 \\ \left(E^{\omega}_{y}\right)^2 \\ 2E^{\omega}_{x}E^{\omega}_{y} \end{bmatrix} , \tag{6}$$

where θ is the angle between the laboratory x and the crystallographic x' axes. Assuming, for example, that the input polarization is fixed along x, one obtains from (6) the field components $E^{2\omega}_{\mathrm{FI-R},x} \propto \cos 3\theta (E^{\omega}_{x})^2$ and $E^{2\omega}_{\mathrm{FI-R},y} \propto \sin 3\theta (E^{\omega}_{x})^2$. Thus, both the amplitude and sign of the reference field from the quartz crystal along a given polarization can be controlled. Consequently, by rotating and translating the quartz plate relative to the sample, one gains full control of the amplitude and relative phase of the reference field.

1.3 Analysis of signal-to-noise ratio

We now consider briefly the signal-to-noise characteristics for homodyne detection [22] and direct detection of SH measurements of the electric field E^0. We treat as the dominant sources of noise in the measurement, the detection shot noise and any incoherent detection noise. For simplicity, we assume that the laser fluctuations are negligible and that there is complete spatial, temporal, and spectral overlap between the field-dependent and field-independent SH radiation. The influence of the laser fluctuation, as well as the degree of partial coherence in the interference of the fields is examined in [16] for the case of a general homodyne measurement.

In this analysis, we derive the relevant signal-to-noise ratio (SNR) for a homodyne measurement, which can be specialized into a direct measurement by taking the limit of no local oscillator. We assume, in accordance with our measurements and common experimental practice, that the SH signals are detected by photon counting techniques. For a given measurement with a specified data collection time, we may then define N_{FI} as the number of counts arising from the field-independent term $\boldsymbol{E}_{\mathrm{FI}}^{2\omega}$, i.e., the local oscillator signal from the sample and the reference source in the absence of the electric field; N_{I} as the number of counts from incoherent noise sources such as photomultiplier dark current, stray light, and circuit noise; and N_{T} as the total number of counts obtained during a measurement. In terms of these quantities, we identify the number of signal counts as

$$N_{\mathrm{S}} \equiv N_{\mathrm{T}} - N_{\mathrm{FI}} - N_{\mathrm{I}}\,, \tag{7}$$

which gives explicitly the field-dependent part of the measured response. It follows from (4) that the number of signal counts obtained in the homodyne measurement is

$$N_{\mathrm{S}} = N_{\mathrm{FD}} + 2\sqrt{N_{\mathrm{FD}} N_{\mathrm{FI}}}\cos\varphi\,, \tag{8}$$

where N_{FD} is the number of counts associated with field-dependent radiation $\boldsymbol{E}_{\mathrm{FD}}^{2\omega}$, i.e., the EFISH signal that arises from the sample. For convenience, we assume that $\cos\varphi \geq 0$ in the ensuing discussion.

The quantity of interest in the SNR calculation is the standard deviation of the number of signal counts, ΔN_{S}. If we assume that the incoherent noise and the field-independent SH count rates are not subject to drift, we may then perform one lengthy and accurate measurement of these quantities. If we perform such measurements then we may use these values to determine the signal counts in a given measurement from the total number of counts without the introduction of any additional error. In this event, $\Delta N_{\mathrm{S}} = \Delta N_{\mathrm{T}}$. The standard deviation ΔN_{T} is governed by the expected Poisson statistics of the total number of counts; hence

$$\Delta N_{\mathrm{T}} = \sqrt{N_{\mathrm{T}}}\,. \tag{9}$$

In this expression and below, symbols for the number of counts such as N_{T} should be interpreted as representing the mean value of the corresponding measured quantity. We may then define the SNR [23] as

$$\mathrm{SNR} \equiv \frac{N_{\mathrm{S}}}{\Delta N_{\mathrm{S}}} = \frac{N_{\mathrm{S}}}{\sqrt{N_{\mathrm{S}} + N_{\mathrm{FI}} + N_{\mathrm{I}}}}\,. \tag{10}$$

Two limits are of particular interest: the case of no local oscillator ($N_{\mathrm{FI}} = 0$) and the case of a strong local oscillator ($N_{\mathrm{FI}} \gg N_{\mathrm{FD}}$). The first situation corresponds to direct detection of the signal; the second, when combined with $\varphi = 0$, corresponds to an ideal homodyne measurement. For the direct measurement, we find immediately that

$$\mathrm{SNR}(N_{\mathrm{FI}} = 0) = \frac{\sqrt{N_{\mathrm{FD}}}}{\sqrt{1 + N_{\mathrm{I}}/N_{\mathrm{FD}}}}\,. \tag{11}$$

For the homodyne measurement in the linearized regime of $N_{\mathrm{FI}} \gg N_{\mathrm{FD}}$ and $\cos\varphi \neq 0$, the corresponding expression reads

$$\mathrm{SNR}(N_{\mathrm{FI}} \gg N_{\mathrm{FD}}) \approx \frac{2\sqrt{N_{\mathrm{FD}}}\cos\varphi}{\sqrt{1 + N_{\mathrm{I}}/N_{\mathrm{FI}}}}\,. \tag{12}$$

A comparison of the direct and homodyne measurement techniques reveals two noteworthy points. First, in the limit where incoherent noise is negligible in both detection schemes, homodyning improves the SNR by a factor of two (for $\varphi = 0$) over that for direct detection. This situation reflects the fact that we measure only the relevant phase component of the SH field in the homodyne scheme. Second, examination of the two denominators of (11) and (12), respectively, $(1 + N_{\mathrm{I}}/N_{\mathrm{FD}})^{-1/2}$ and $(1 + N_{\mathrm{I}}/N_{\mathrm{FI}})^{-1/2}$, demonstrates the well-known advantage of homodyne detection in the presence of an incoherent noise background. By the choice of a sufficiently strong optical bias field in the homodyne measurement, we may, in principle, reduce the factor $N_{\mathrm{I}}/N_{\mathrm{FI}}$ to an arbitrary extent. This is equivalent to eliminating the degradation of the SNR associated with incoherent noise sources. From a practical standpoint, a homodyne measurement should allow one to reduce the typical stringent requirements on ambient light levels or photomultiplier dark current typically associated with photon counting of weak signals. The homodyne method may also enhance the attractiveness of detectors, such as avalanche or p-i-n photodiodes, which exhibit favorable quantum efficiency but are usually associated with higher electronic noise than photomultiplier tubes [24].

For completeness, we consider the case where $N_{\mathrm{FI}} \gg N_{\mathrm{FD}}$ and $\varphi = \pi/2$. In this situation, the interference between the signal and the reference is lost so that an increase in N_{FI} simply increases the corresponding shot-noise in the detected signal and decreases the corresponding SNR. The explicit expression for the SNR is

$$\mathrm{SNR}(N_{\mathrm{FI}} \gg N_{\mathrm{FD}};\, \varphi = \pi/2) \approx \frac{\sqrt{N_{\mathrm{FD}}}}{\sqrt{1 + (N_{\mathrm{FI}} + N_{\mathrm{I}})/N_{\mathrm{FD}}}}\,. \tag{13}$$

In this instance, as N_{FI} is increased, the SNR decreases monotonically. It approaches zero for large values of N_{FI} where the shot noise of the field-independent contribution completely overwhelms the signal. This relation, as well as the φ dependence in (12), demonstrates the sensitivity of the SNR to the relative phase between the SH signal and reference fields, and highlights the importance of maintaining an in-phase relationship between these two waves.

We now extend the SNR calculations of the direct and homodyne schemes to the corresponding measurements performed with differential detection. In such measurements, the electric field $\boldsymbol{E}^0$ being probed is turned on and off at some specified modulation frequency. The SH signals are then accumulated for both the on and off states, and the results are subtracted from one another to yield the field-dependent response. A differential detection scheme of this sort is attractive in cases where the average count rates from either the SH signal or the incoherent background experience drift. The assumption made above about our ability to determine N_{FI} and N_{I} with high accuracy in a single long measurement is then invalid, and the differential technique may be favored or required. The differential detection scheme will reduce, for example, the influence of laser noise and drift, which have not been included in our analysis of the SNR.

For differential detection with square wave modulation and equal on and off cycles, we find the following expressions for the cases parallel to those of (11)–(13):

$$\mathrm{SNR}^{\mathrm{Diff}} = \frac{\sqrt{N_{\mathrm{FD}}}}{\sqrt{1+2N_{\mathrm{I}}/N_{\mathrm{FD}}}}\,, \tag{11′}$$

$$\mathrm{SNR}^{\mathrm{Diff}}(N_{\mathrm{FI}} \gg N_{\mathrm{FD}}) \approx \frac{\sqrt{2N_{\mathrm{FD}}}\cos\varphi}{\sqrt{1+N_{\mathrm{I}}/N_{\mathrm{FI}}}}\,, \tag{12′}$$

and

$$\mathrm{SNR}^{\mathrm{Diff}}(N_{\mathrm{FI}} \gg N_{\mathrm{FD}};\, \varphi=\pi/2) \approx \frac{\sqrt{N_{\mathrm{FD}}}}{\sqrt{1+2(N_{\mathrm{FI}}+N_{\mathrm{I}})/N_{\mathrm{FD}}}}\,, \tag{13′}$$

where the number of counts in these expressions should now be interpreted as corresponding to a duty cycle of $1/2$. The degradation in the SNR in these relations compared with the previous detection scheme results from the presence of additional variance in the background signals during the off cycle without a concomitant increase in the strength of the signal. Indeed we can obtain these formulas for differential detection simply by making the substitution $N_{\mathrm{FI}} \to 2N_{\mathrm{FI}}$ and $N_{\mathrm{I}} \to 2N_{\mathrm{I}}$ in the denominator of (10).

Let us examine these equations. In the limit of negligible incoherent background, we note the following: (1) For direct detection, we obtain $\mathrm{SNR}^{\mathrm{Diff}} = \sqrt{N_{\mathrm{FD}}}$, which is expected for a shot-noise-limited signal; and (2) for homodyne detection with $\varphi = 0$, there is now only a factor of $\sqrt{2}$ improvement over the direct measurement, in contrast to a factor of 2 improvement using a non-differential measurement. In the limit of a large incoherent background, (11′) becomes $\mathrm{SNR}^{\mathrm{Diff}} = N_{\mathrm{FD}}/\sqrt{2N_{\mathrm{I}}}$, also as expected. More generally, we see that the SNR for a homodyne measurement always exceeds that for the corresponding direct measurement by a factor of $\sqrt{2}$, but this enhancement factor may be much greater when large incoherent noise sources are present.

Before leaving this topic, we would like to recall that the importance of laser noise increases as one approaches a more and more idealized homodyne measurement, i.e., in the limit of $N_{\mathrm{FI}}/N_{\mathrm{FD}} \to \infty$. This regime provides optimal linearization and optimal suppression of incoherent noise, but makes the requirement for laser noise increasingly severe, as the fractional modulation induced by the signal becomes increasingly weak. Thus, from a practical point of view, the stability and noise characteristics of the pump laser source influence the choice of the desired optical bias field. It is necessary to obtain a proper balance between linearity and excessive sensitivity to laser noise.

Another limitation to be considered concerns the degree of interference between the signal and reference fields. The quality of the interference can be degraded by imperfect spatial, temporal, or spectral overlap of the two fields. The non-overlapping components of the fields can be thought of as having a relative phase of $\pi/2$, since they do not interfere at the detector. It follows from (13) and (13′) that the overall SNR will be reduced, to a greater or lesser degree depending on the strength of the non-interfering component of the reference field. The same qualitative conclusion may be reached by consideration of phase shifts $\varphi > 0$ in (12) and (12′).

2 Experimental conditions

Figure 1 illustrates the experimental setup schematically. The source for the SH probe is a Ti:sapphire laser producing pulses of 70 fs duration at a wavelength of 770 nm and a repetition rate of 80 MHz. In the SH measurements, the laser beam, with an average power of 200 mW, impinges on the silicon sample at a 3° incidence angle and is focused to a spot size of 20 μm. The reflected fundamental and SH beams are then recollimated. After going through a filter that transmits the SH while blocking the fundamental, the SH radiation passes through an analyzer and is detected by a cooled photomultiplier tube. The photomultiplier output is processed with gated photon counting electronics. The polarization configuration of this experiment was *s*-polarized fundamental radiation and *s*-polarization for the detected SH radiation. This configuration eliminates the field-independent surface and bulk background terms, as discussed in Sect. 1.1.

Our sample was a silicon-on-sapphire wafer on which aluminum strip lines were deposited. The electrode geometry is shown in the inset of Fig. 1. It consists of lines with a 30 μm spacing, but with a narrowed gap of 5 μm width in the probing region. The sample was treated by a sequence of ion-implantation steps, which rendered the 0.6 μm-thick silicon epilayer nearly isotropic and served to reduce the carrier lifetime to less than 1 ps [25]. The reduced carrier lifetime significantly decreases the importance of screening of the bias field associated with carriers produced by the laser pulse [11]; it also eliminates the cumulative effects that arise from charge trapping at the SiO_2 layer [26]. In addition, the ion-implantation of the sample leads to ohmic contact be-

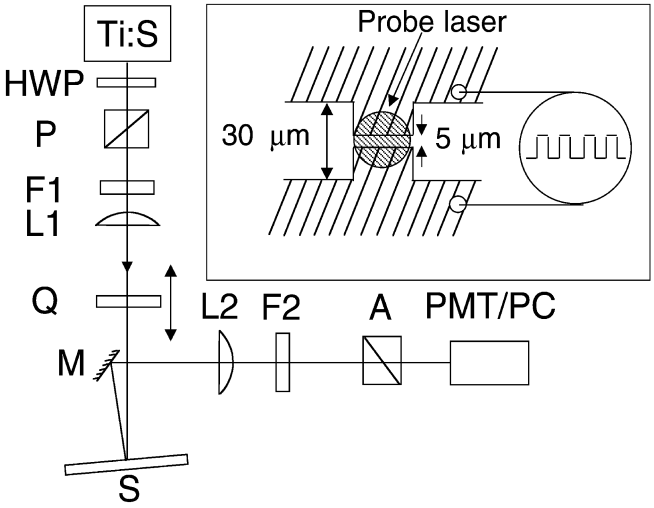

Fig. 1. Main panel: Experimental setup. A Ti:sapphire laser (Ti:S) provides pulses of 770 nm wavelength at 80 MHz repetition rate and 70 fs pulsewidth. The beam passes through a half-wave plate (HWP), a polarizer (P), a filter (F1) that blocks spurious SH radiation but transmits the fundamental light, and is focused by the lens (L1), through a quartz plate (Q), to the sample (S) at a 3° incidence angle. For a direct measurement, Q is removed. The reflected total SH radiation from both Q and S are redirected by mirror (M) through a collimating lens (L2) and a filter (F2) that blocks the fundamental, but transmits the SH beam. The transmitted SH radiation goes through an analyzer (A) and is then detected by a photomultiplier with gated photon counting electronics (PMT/PC). Inset: Details of probing geometry. A pair of aluminum electrodes on an ion-implanted silicon-on sapphire substrate, provides the electric field being probed. This field is modulated at 100 kHz frequency and detected differentially

tween the metal and silicon. The sample was oriented so that the electric field $\boldsymbol{E}^0$ induced by the applied bias voltage V on the electrodes was perpendicular to the plane of incidence of the probe laser, i.e., parallel to the polarization of the probe beam. The bias voltage, which was modulated at 100 kHz, could be varied between ± 15 V. The count rates for the SH signal in the on and off states were collected separately and subtracted in a differential measurement, as described above. For each bias voltage, the data collection time was 8 s, with half the measurement with the voltage on and half without the bias.

For the homodyne measurements, we employed a z-cut quartz plate of 250 μm thickness to produce the reference SH radiation. The quartz plate was inserted normal to the laser beam between the focusing lens and the sample. This location for the quartz reference provided an appropriate signal strength for the homodyne measurement. While the placement of the quartz plate after the focusing lens yields some change in the amplitude of the reference beam as the reference beam is displaced to optimize the relative phase of the SH beams, it is desirable to have as little dispersive material as possible between the quartz reference and the sample. This situation is necessary to avoid degraded interference between the signal and the reference beams associated with temporal shifts induced by the group velocity dispersion between the fundamental frequency (giving rise to the SH radiation from the sample) and the SH frequency (associated with the SH radiation from the quartz plate). A related consideration dictated our choice of a *thin* quartz plate. For a thicker plate, dissimilar degrees of phase matching for the different frequency components of the fundamental beam will lead to distortion of the SH pulse and to a degraded quality of interference between the sample and reference SH beams.

3 Results and discussion

In Fig. 2, we present data for measurement of the electric field E^0 by direct detection of the EFISH radiation. We observe the predicted quadratic dependence of the SH intensity on E^0, which is proportional to the applied bias voltage V across the electrodes on the silicon sample. This measurement was performed with s-polarized input radiation and detection of the s-polarized SH field. For this configuration, as discussed above, no field-independent SH radiation is expected and the minimum of the parabolic variation of SH with electrical bias should be centered at $V = 0$. This is essentially the behavior observed in the data of Fig. 2. The slight shift of the minimum of the parabola toward positive voltages maybe be explained by the existence of a residual SH reference field. Such a field may arise from imperfect alignment of the input and output polarizations, since the surface and bulk quadrupole terms of the sample may then produce SH radiation. Alternately, this slight shift could be attributed to some degree of non-ohmic behavior at the semiconductor electrode interfaces and the concomitant presence of weak, built-in electric fields in the sample. In contrast to these effects, an incoherent SH source merely adds an offset to the measured SH while keeping the measured minimum SH signal at zero bias voltage.

We now turn to measurements in which we have introduced a well-defined reference SH field that is independent of the sample bias. As indicated in the previous section, we

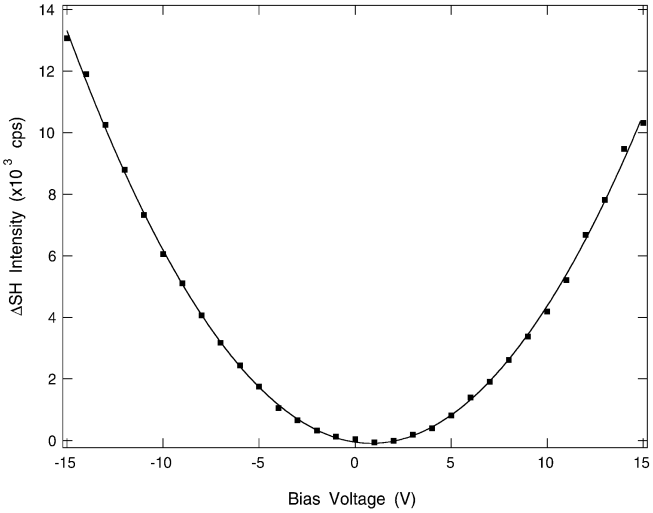

Fig. 2. Direct detection of SH dependence on the bias voltage with the bias-independent background subtracted in a differential measurement. The *solid curve* is a quadratic fit to the experimental points. The SH signal is expressed in terms of the count rate during the on-state of the modulation cycle

make use of a thin quartz plate for this purpose. Figure 3 shows the resulting interference between this reference signal and the field-induced signal from the sample as a function of the displacement of the quartz plate along the path of the probe laser beam. For this measurement, the amplitude of the quartz reference was adjusted so that the interference between the two signals was optimal. The interference signal is normalized with respect to the reference signal alone, i.e., without a field-induced signal from the sample. This normalization was performed to account for the varying SH field strength from the quartz plate as it is translated along the focused beam path. The data are fit using (4) and yield an oscillation period of $\Delta L = 47 \pm 1$ mm, in excellent agreement with the predicted period of 46 mm based on the dispersion of air at the relevant wavelengths. The deviation in the fit can be attributed to the changing amplitude of the SH radiation from the quartz reference as it is translated along the path of the focused probe laser beam. With careful optimization, a modulation depth of 80–90% was attainable in these interference measurements.

To illustrate the importance of the proper choice of relative phase between the sample and reference fields, we first examine the behavior when these fields are in quadrature, corresponding to $\varphi = \pi/2$. From the data in Fig. 3, this condition is achieved when the quartz plate is positioned at $l \approx 21$ mm. In this measurement, the quartz plate was rotated, in accordance with (6), to yield a field much larger than that of the sample. Here, the number of field-independent SH counts was $N_{\mathrm{FI}} \approx 10^5$, for a 1 s half cycle of data collection time. For this quadrature phase relation, no interference between the two signals occurs. Thus, a parabolic variation of the measured SH signal with the electric field is expected, according to (4). The experimental data of Fig. 4 illustrates this behavior. The slight shift in the minimum of the parabola is attributed to a minor deviation from $\varphi = \pi/2$ that yields a residual offset in (4). (We note that the SH signal obtained in Fig. 4 is only 75% as large as that shown in Fig. 2. This decrease arises primarily from the transmission loss of the fundamental beam as

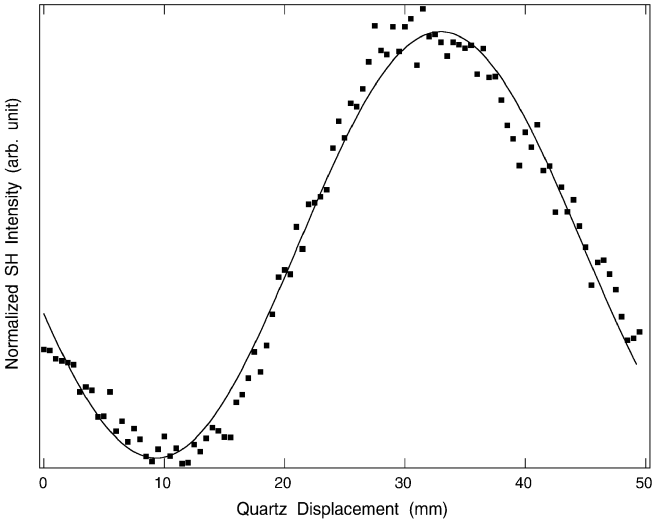

Fig. 3. Interference between the quartz SH field and the sample EFISH field as a function of the quartz displacement along the SH probe beam. The *solid curve* is the fit to the experimental points, according to (4). The fit yields a modulation period of 47 mm

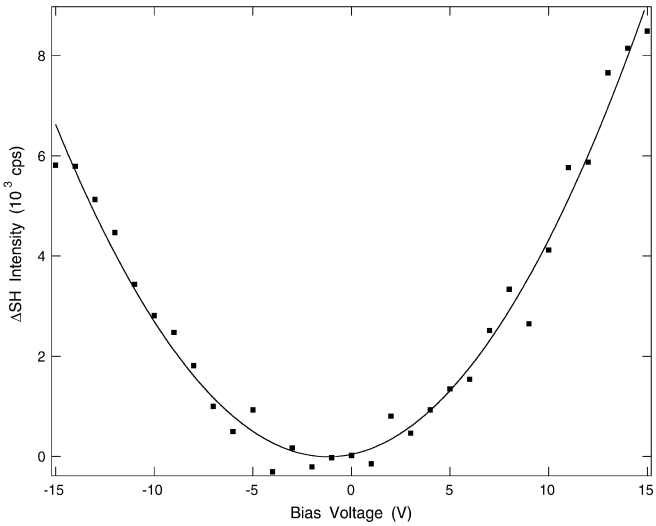

Fig. 4. SH dependence on the bias voltage in the presence of a large quartz SH field that has a quadrature phase relationship ($\varphi = \pi/2$) with the sample EFISH signal. The *solid curve* is a quadratic fit to the experimental points. Note that the bias-independent background has been subtracted and the SH intensity is expressed in terms of the count rate during the on-state of the modulation cycle

it passes through the quartz plate.) While the form of the bias dependence for the case of the background-free measurement (Fig. 2) and the case of a reference field in quadrature to the EFISH field (Fig. 4) are essentially identical, the SNR of the latter is degraded. This situation arises because the addition of a large reference field in quadrature phase is equivalent to adding incoherent noise in the direct measurement scheme [(13) and (13′)]. Indeed, analysis of the data of Figs. 2 and 4 indicates that the presence of the quadrature reference field reduces the SNR by a factor of ~ 4.

Figure 5 demonstrates homodyne detection of the original signal shown in Fig. 2. This provides the desired linear dependence of the measured SH intensity on the electric field strength E^0 being probed. To achieve the appropriate characteristics in the homodyne measurement, we adjusted both the amplitude and phase of the SH reference field as prescribed by (4). First, to optimize the interference, the quartz plate was translated until the relative phase between the sample and reference fields corresponded to $\varphi = 0$ ($l \approx 33$ mm in Fig. 3). The quartz plate was then rotated about its axis to adjust the amplitude of the SH reference field to yield $N_{\mathrm{FI}} \approx 10^5$. The data in Fig. 5 show the approximately linear variation of the SH signal with electric field E^0, as controlled by the bias voltage applied to the sample electrodes. This behavior stands in obvious contrast to that exhibited in Figs. 2 and 4 for the background-free and quadrature reference cases, respectively.

To evaluate the linearity of the data, we fit these results using the full parabolic expression for the electric-field dependence of the SH intensity, as given by (4). For bias voltages less than 1 V, as shown in the inset, this dependence is linear to high accuracy. For larger bias voltages, as shown in the main panel, some deviation from linearity is evident. To illustrate this behavior more explicitly, consider a bias of 10 V. At this bias, $N_{\mathrm{S}} \approx 2.5 \times 10^4$, which 25% of the field-independent value of $N_{\mathrm{FI}} \approx 10^5$. From (4a) and (8), we then infer that $E^{2\omega}_{\mathrm{FD}}/E^{2\omega}_{\mathrm{FI}} = 1/8$. We also see that the magnitude of the last term in (4), which depends linearly on $E^{2\omega}_{\mathrm{FD}} \propto E^0$, is 16 times larger than the first term, which depends quadratically on $E^{2\omega}_{\mathrm{FD}}$. Hence, some departure from linearity is expected. Another point of interest concerns the degree of interference between the field-induced and reference radiation. By examining (4a), we find that the slope of the SH intensity dependence on the field $E^{2\omega}_{\mathrm{FD}} \propto E^0$ is directly related to the degree of interference. To evaluate the expected slope of the signal for the case of perfect interference with $\varphi = 0$, the relative strengths of the two fields $E^{2\omega}_{\mathrm{FI}}$, and $E^{2\omega}_{\mathrm{FD}}$, or their corresponding number of counts, N_{FI} and N_{FD}, should be known.

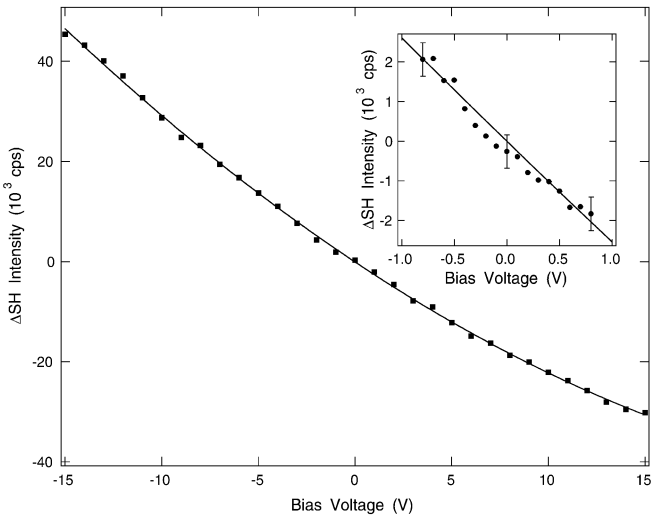

Fig. 5. Main panel: Linearization of the SH intensity dependence on the bias voltage using the homodyne detection scheme. The EFISH signal from the sample is mixed with a large, in-phase ($\varphi = 0$) SH reference field from the quartz plate. The *solid curve* is a quadratic fit to the experimental points to account for the curvature at larger voltages. Note that the bias-independent background has been subtracted and the SH intensity is expressed in terms of the count rate during the on-state of the modulation. Inset: Dependence of SH on bias for small voltages. The *error bars* show the standard deviation for a data collection time of 8 s. The *solid line* is the same fitting curve used in the main panel

The number of counts N_{FD} is obtained from Fig. 4, which does not depend on the degree of interference. Using (8), we can then predict the slope. We find that the experimental slope from Fig. 5 is only 65% of the expected slope. This reflects imperfect interference between the EFISH and field-independent SH radiation.

We now compare the SNR in the homodyne (Fig. 5) and direct detection (Fig. 2) schemes. From an analysis of the χ^2-parameter for the fits to Figs. 5 and 2, we can estimate the typical standard deviation of the experimental data. We obtain the ratio of $\Delta N_S(\text{homodyne})/\Delta N_S(\text{direct}) = 4.4$. To compute the relative SNR, we use the value of the signal strength for bias of 10 V. We find a ratio of $\text{SNR(homodyne)}/\text{SNR(direct)} \approx 1.1$. This result is roughly in line with the expected improvement in the SNR by a factor of at least $\sqrt{2} \approx 1.4$, from (11′) and (12′). The reduced relative SNR seen experimentally for the homodyne measurement is attributed primarily to the imperfect interference between the reference and signal fields, as discussed above. Another factor that may contribute to the degradation of the SNR for the homodyne measurement is the effect of fluctuations of the probe laser, as discussed at the end of Sect. 1.2.

We now evaluate the electric-field sensitivity of the homodyne measurement. The data in the inset of Fig. 5 show experimental error bars for a data collection time of 8 s. From the slope of the variation of the SH intensity with the applied bias field, we may infer an electric-field sensitivity of $\sim 270\,\text{V/cm}$, corresponding to one standard deviation in the SH data. Equivalently, we obtain $E^0_{\min} \sim 760\,\text{V/cm/Hz}^{1/2}$, which is close to the calculated minimum detectable field of $E^0_{\min} \sim 280\,\text{V/cm/Hz}^{1/2}$. To deduce this minimum detectable electric field, we set $\text{SNR}^{\text{Diff}} = 1$ in (12′). This yields $N_{FD} = 1/2$, provided that the incoherent background is negligible. In the experiment, we measured $N_{FD} \approx 2.5 \times 10^3$ counts for a total data collection time of 1 s (0.5 s in the on-state and 0.5 s in the off-state) at an electric field strength of 20 kV/cm. Since $N_{FD} \propto (E^0)^2$, the minimum detectable field (corresponding to $N_{FD} = 1/2$) is then found to be $E^0_{\min} \sim 280\,\text{V/cm/Hz}^{1/2}$. This quantity can be further lowered by optimizing the geometry (such as focusing and incidence angle), laser properties (such as pulse energy, pulsewidth, and wavelength) and material parameters (such as $\chi^{(3)}$). As an example, consider the experimental parameters used in the experiment of Nahata et al. [14]. By employing a tighter focusing and shorter laser pulses, the authors observed a count rate for N_{FD} that exceeded the corresponding value in our experiments by a factor of 8. Hence, the minimum detectable field will be reduced by a factor of $\sqrt{8}$ to $E^0_{\min} \sim 100\,\text{V/cm/Hz}^{1/2}$.

4 Summary

In this paper we have examined the application of the homodyne detection scheme to measurements of electric fields through the process of electric-field induced second-harmonic generation. In this approach, an optical reference field at the second-harmonic frequency is generated that is large compared to and in-phase with the field-induced SH radiation. By mixing these two SH fields, we obtain a SH intensity that varies linearly with the strength of the electric field being probed. The approach makes calibration of the electric field strengths easy and yields information on the sign the electric field directly. Experiments demonstrating these properties were performed for silicon structures with in-plane static fields imposed by metal electrodes. The reference signal was provided by a quartz plate, which could be adjusted to generate a local-oscillator signal of arbitrary phase and amplitude. The results of the homodyne measurement scheme were compared with the corresponding measurement for direct (background-free mode) detection and for the case where the reference field was in quadrature with the signal, both of which exhibited the expected quadratic variation of the SH intensity with the electric field strength.

An analysis of the signal-to-noise characteristics for the direct and homodyne measurements was presented. It is found that an improvement in the shot-noise limited performance is expected for the homodyne measurement scheme, as well as a suppression of noise associated with incoherent background signals. The actual degree of improvement under experimental conditions will depend on quality of the interference between the signal and reference beams, and may be degraded if excessive laser noise is present. While the full predicted improvement in the signal-to-noise was not achieved experimentally, the homodyne detection scheme provided a sensitivity to electric fields on the order of 100 V/cm for integration times of seconds. Significant improvements in field sensitivity through optimization of the experimental geometry, laser properties, and material parameters can be anticipated. We are presently applying the homodyne detection scheme to map the vector character of the electric fields in semiconductor structures and to probe ultrafast electrical transients.

Acknowledgements. The authors would like to thank Georg Reider and Ajay Nahata for useful discussions. This work was funded by the AFOSR (grant F49620-98-1-0137), the NSF (grant CHE-96-12294), and the ISEP (grant DAAG55-97-1-0166).

References

1. See, for example, the articles in Appl. Phys. A **59**, (4–6) (1994), and **60**, (1, 2) (1995), and articles in this issue
2. T.F. Heinz: In *Nonlinear Surface Electromagnetic Phenomena*, ed. by H.-E. Ponath, G.I. Stegeman (North-Holland, Amsterdam 1991) p. 353; G.A. Reider, T.F. Heinz: In *Photonic Probes of Surfaces*, ed. by P. Halevi (Elsevier, Amsterdam 1995) p. 413
3. R.W. Terhune, P.D. Maker, C.M. Savage: Phys. Rev. Lett. **8**, 404 (1962)
4. C.H. Lee, R.K. Chang, N. Bloembergen: Phys. Rev. Lett. **18**, 167 (1967)
5. O.A. Aktsipetrov, A.A. Fedyanin, V.N. Golovkina, T.V. Murzina: Opt. Lett. **19**, 1450 (1994)
6. J.I. Dadap, X.F. Hu, M.H. Anderson, M.C. Downer, J.K. Lowell, O.A. Aktsipetrov: Phys. Rev. B **53**, R7607 (1996); O.A. Aktsipetrov, A.A. Fedyanin, J.I. Dadap, M.C. Downer: Laser Phys. **6**, 1142 (1996)
7. P. Godefroy, W. de Jong, C.W. van Hasselt, M.A.C. Devillers, Th. Rasing: Appl. Phys. Lett. **68**, 1982 (1996)
8. J. Qi, M.S. Yeganeh, I. Koltover, A.G. Yodh, W.M. Theis: Phys. Rev. Lett. **71**, 633 (1993); T.A. Germer, K.W. Kolasinski, J.C. Stephenson, L.J. Richter: Phys. Rev. B **55**, 10 694 (1997)
9. See, for example, the reviews by K.B. Eisenthal: Chem. Rev. **96**, 1343 (1996); R.M. Corn, D.A. Higgins: Chem. Rev. **94**, 107 (1994); G.L. Richmond, J.M. Robinson, V.L. Shannon: Prog. Surf. Sci. **28**, 1 (1988)
10. J.M. Lantz, R.M. Corn: J. Phys. Chem. **98**, 9387 (1994)
11. J.I. Dadap, P.T. Wilson, M.H. Anderson, M.C. Downer, M. ter Beek: Opt. Lett. **22**, 901 (1997)

12. W. de Jong, A.F. van Etteger, C.A. van 't Hof, P.J. van Hall, Th. Rasing: Surf. Sci. **352**–**354**, 807 (1996)
13. C. Ohlhoff, C. Meyer, G. Lüpke, T. Löffler, T. Pfeifer, H.G. Roskos, H. Kurz: Appl. Phys. Lett. **68**, 1 (1996); C. Ohlhoff, G. Lüpke, C. Meyer, H. Kurz: Phys. Rev. B **55**, 4596 (1997)
14. A. Nahata, T.F. Heinz, J.A. Misewich: Appl. Phys. Lett. **69**, 746 (1996)
15. A. Nahata, T.F. Heinz: Opt. Lett. **23**, 67 (1998)
16. P. Thiansathaporn, R. Superfine: Opt. Lett. **20**, 545 (1995)
17. M. Cernusca, M. Hofer, G.A. Reider: J. Opt. Soc. Am. B **15**, 2476 (1998)
18. See, for example, R. Stolle, G. Marowsky, E. Schwarzberg, G. Berkovic: Appl. Phys. B **63**, 491 (1996) and references therein
19. O.A. Aktsipetrov, I.M. Baranova, Yu. A. Il'inskii: Sov. Phys. JETP **64**, 167 (1986); J.E. Sipe, D.J. Moss, H.M. van Driel: Phys. Rev. B **35**, 1129 (1987)
20. B. Edlen: Metrologia, **2**, 71 (1966)
21. J. Jerphagnon, S.K. Kurtz: J. Appl. Phys. **41**, 1667 (1970)
22. See, for example, A. Yariv: *Introduction to Optical Electronics* (Holt, Rinehart and Winston, New York 1971)
23. The relationship between the definitions of the SNR of this work and the SNR used in [16] is $(\mathrm{SNR[this\ work]})^2 = \mathrm{SNR}$ [16], where the latter SNR is expressed in terms of signal and noise power ratios
24. J. Chen, S. Machida, Y. Yamamoto: Opt. Lett. **23**, 676 (1998)
25. F.E. Doany, D. Grischkowsky, C.C. Chi: Appl. Phys. Lett. **50**, 460 (1987)
26. J. Bloch, J.G. Mihaychuk, H.M. van Driel: Phys. Rev. Lett. **77**, 920 (1996)